Molecular dynamics of shock-wave induced structural changes in silica glasses

F. Barmes
Centre Européen de Calcul Atomique et Moléculaire, 46, allée d'Italie, 69007 Lyon, France

L. Soulard
CEA-DAM Ile-de-France, Boite Postale 12, 91680 Bruyères-le-Châtel, France

M. Mareschal
Faculté des Sciences, Université Libre de Bruxelles, CP231, Boulevard du Triomphe B1050, Brussels, Belgium
(Received 17 January 2006; revised manuscript received 9 May 2006; published 16 June 2006)

We seek to model the shock wave induced structural changes in silicate glass at the atomic scale. We use both direct shock propagation with nonequilibrium molecular dynamics (NEMD) and bulk simulations in the Hugoniot ensemble to characterize the structure and topology of the shocked glass. Despite the lack of long-range interactions in our model, the close agreement between our structures and those obtained by experimental and simulation studies alike underlines the importance of the role played by first neighbor interactions on the structure of silicate glass. The results obtained from this study show that, in agreement with experimental work, the structure and topology of the shock-induced densified phase is unique in its structure as can be revealed by medium-range order measurements. The modifications include a reduction of the average tetrahedra size and an increase in the proportion of 3–4 and 8–10 membered Si-rings. Application of a Hugoniostat method based on constraint dynamics shows near-perfect agreement with the NEMD results. Besides validating the former method, this opens the prospect of studying shock-induced effects at a fraction of the cost required to run large scale shock simulations while using much more complicated potentials and setups.

DOI: 10.1103/PhysRevB.73.224108 PACS number(s): 62.50.+p, 47.40.Nm, 61.43.Fs

I. INTRODUCTION

High power lasers are used to achieve extreme temperature and pressure conditions. During such experiments, deterioration of the optics due to the passage of the laser has been observed in the form of small craters at the back of the lenses.[1,2] It is believed that these craters originate from the absorption of the laser by defects which create a dense absorbing plasma. The induced temperature rise in turn triggers the propagation of a mechanical shock wave creating regions of permanently densified glass.[3]

Experimental work on shock compression shows the creation of a densified phase upon propagation of a shock wave through silica glass.[4] Kubota *et al.*[5,6] have used molecular dynamics to propagate shock waves with up to 2.0 Km/s piston velocity through slabs of up to 240×10^3 atoms. The authors show drastic shock induced modifications in the structure and topology of the SiO_2 network. It has also been shown that the structure of the resulting densified phase is unique as can be revealed by medium-range order measurements such as the ring size distribution.[7–9]

Despite the major increase in the available computer power which allows simulation of several hundred million atoms, nonequilibrium molecular dynamics (NEMD) simulations of shocked materials still represent a computationally major undertaking. This is mainly due to the large system sizes needed to achieve a steady shock front; additionally a non-negligible part of the total simulation time is spent calculating the trajectories of particles in the unshocked region. Another NEMD method has been used in Ref. 10 where the simulation box consists of a moving window which follows the shock front. The method achieves an accurate description of the shock induced effects provided steady shock waves are obtained. Alternatively, to address the system size problem, several groups have attempted to construct a method where equilibrium simulations are performed on bulk systems in the Hugoniot ensemble. Such a method allows usage of much smaller systems to achieve results equivalent to those obtained with NEMD. The first such method (GNVHug) was proposed by Soulard[11] and uses the Gauss principle of least constraints to integrate the equations of motions and constrain the system on the Hugoniot. This method presents the double advantage of reaching equilibrium very rapidly $[\mathcal{O}(10^{-13})\mathrm{s}]$ and guaranteeing that the system obeys the Hugoniot relations at all times. The method was applied to the simulation of shocked liquid argon and nitromethane[11,12] and has shown good agreement with NEMD simulations. An alternative approach was proposed by Maillet *et al.*[13] which uses a Nosé-Hoover-like method to couple the system, instantaneously, uniaxially, and homogeneously compressed to the shock density, with a thermostat to achieve the final Hugoniot state. Applied to the shock deformation of Lennard-Jones crystals along the $\langle 100\rangle$ direction, the method has shown to reproduce both the Hugoniot curve and the shock induced defect structure. This method was later extended to *ab initio* molecular dynamics to obtain the shock Hugoniot of tin up to 200 GPa.[14] Answering the criticism that the instantaneous compression of the system can lead to unrealistically large temperatures and stresses, Ravelo *et al.*[15] improved the uniaxial Hugoniostat by adding a strain-rate dynamical variable which acts as a piston. The method allows gradual compression of the system to the shock density and therefore a more natural evolution of both

the temperature and stress. Applied to the calculations of the Hugoniot of Lennard-Jones crystals equivalent to those performed in Ref. 13, the method improves the agreement with NEMD, especially for large compressions.

In this paper, we seek to model the shock induced structural changes in silicon dioxide at the atomic scale. To this end, after validating that our model achieves an accurate description of the glassy state of silicon dioxide, we use NEMD simulations to characterize precisely the structure induced by a mechanical shock wave. We then apply the GNVHug method and show this gives very good agreement with the NEMD results. The remainder of this paper is organized as follows. In Sec. II we present the potential used to describe the interatomic interactions in silicon dioxide. In Sec. III, we describe the methods and results obtained to create and analyze a bulk system of silicon dioxide in the glass phase in order to check our potential leads to an appropriate structure before shocking it. In Sec. IV, we turn on to the study of the structural changes induced by the propagation of a mechanical shock wave using NEMD simulations, while Sec. V concentrates on obtaining similar results with the Hugoniostat. Section VI concludes this work with a discussion of the results drawn from this work and proposes some directions for future developments.

II. THE INTERMOLECULAR POTENTIAL

Accurate description of silicate glass is not in principle an easy task. Ideally the interatomic potential should include Coulombic interactions, and an appropriate method to take the long-range forces into account (e.g., Ewald summation) and also include dynamic charges. Several intermolecular potentials that successfully describe the behavior of silicon dioxide in the glass phase have been built over the years.[16] Among the most widely used, is the so-called BKS potential developed by van Beest *et al.*[17] and the three body potential of Vashishta *et al.*[18] which we will refer to as the VKRE potential hereforth. We choose to use the BKS potential, as it allows for faster simulation than the more complicated three-body form of the VKRE potential while leading to similar results; the three body information necessary to create the tetrahedra network in silicon dioxide is not lost with the BKS potential, but is implicitly present by the choice of the potential parameters derived from the cluster model of van Beest *et al.*[17]

The BKS potential is a two-body potential based on the Buckingham potential with an added Coulombic term. The potential describes the interaction between two atoms i and $j=\{\mathrm{Si},\mathrm{O}\}$ separated by $\mathbf{r}_{ij}=r_{ij}\hat{\mathbf{r}}_{ij}$, the interatomic vector as follows:

$$\mathcal{V}^{\mathrm{BKS}}=\frac{A_0 q_i q_j}{r_{ij}}+A_{ij}e^{-B_{ij}r_{ij}}-\frac{C_{ij}}{r_{ij}^6}, \tag{1}$$

with $A_0=1/(4\pi\epsilon_0)=2.307\times10^{-28}$ J/m. Values for the A_{ij}, B_{ij}, and C_{ij} parameters are taken from Ref. 17 and recalled here in Table I.

Buckingham-like potentials have the unphysical property of diverging to minus infinity at small interatomic distances which can be disastrous at high temperatures where atoms have the kinetic energy to overcome the potential barrier and fuse together. Several methods have been employed to correct for this behavior. Vollamyr *et al.*[19] replaces the BKS potential with a harmonic form for $r^0_{\mathrm{SiO}}\leqslant 1.1936$ Å and $r^0_{\mathrm{OO}}\leqslant 1.439$ Å. Another method is that of Guissani and Guillot[20] or Coluzzi and Verrocchio[21] where 18–6 and 24–6 Lennard-Jones potentials are, respectively, added to the BKS form. Here we choose to follow the former method and replace the BKS potential with a second order polynomial $p(r)$ for $r<r^0$.

TABLE I. Numerical values of the BKS potential parameters as given by van Beest *et al.* (Ref. 17).

	A_{ij} (J)	B_{ij} (m^{-1})	C_{ij} (Jm^6)
O-O	2.225×10^{-16}	2.760×10^{10}	2.804×10^{-77}
Si-O	2.884×10^{-15}	4.873×10^{10}	2.139×10^{-77}
Si-Si	0.0	0.0	0.0

We also make the assumption that the structure of SiO_2 is essentially controlled by the interactions within the shell of first neighbors and as a result we cut and shift the potential for $r>r_c$. This assumption comes from the argument that since silicate glass is essentially a random continuous network of SiO_2 tetrahedra, controlling the shape of an individual tetrahedra and its relative position with respect to its first neighbors is sufficient to recover medium and long-range order.

It should be noted that the effects on the structural and dynamic properties of cutting the Coulombic part of the potential are different than those described by Jund *et al.*[22] Here we simply cut and shift the potential for $r>r_c$ but keep all contributions to the potential, including the Coulombic term, below the cutoff distance which is 3.6 times greater than the average Si-O distance. Jund *et al.*, on the other hand, studied the effect of gradually removing the Coulombic part of the potential at *all distances*. A quantitative study on the effects of the long range forces on the structure of silicate glasses is under way and will be the subject of a future publication.[23] In the light of the preliminary results obtained (not shown here), we are, however, confident that the long-range forces effect is negligible in the structural properties of silicate glass.

Preliminary results (not shown here) however, seem to confirm our approximation for the structural properties.

The final form of the potential used here is expressed as follows:

$$\mathcal{V}=\begin{cases} p(r)=a_{ij}r^2+b_{ij}r+c_{ij} & r_{ij}\leqslant r^0_{ij} \\ \mathcal{V}_c^{\mathrm{BKS}} & r^0_{ij}<r_{ij}\leqslant r_c \\ 0 & r_{ij}>r_c, \end{cases} \tag{2}$$

with

$$\mathcal{V}_c^{\mathrm{BKS}}=\mathcal{V}^{\mathrm{BKS}}(r)-\mathcal{V}^{\mathrm{BKS}}(r_c)-(r-r_c)\frac{d\mathcal{V}^{\mathrm{BKS}}(r_c)}{dr},$$

the cut and shifted version of the potential. We set $r_c=6$ Å, $r^0_{\mathrm{SiO}}=1.5$ Å, and $r^0_{\mathrm{OO}}=2.0$ Å. The coefficients of $p(r)$ are cal-

TABLE II. Numerical values used for the coefficient of the polynomial functions.

	a_{ij} (J/m^2)	b_{ij} (J/m)	c_{ij} (J)
O-O	1.510×10^{2}	-7.925×10^{-8}	1.100×10^{-17}
Si-O	3.413×10^{2}	-9.361×10^{-8}	3.925×10^{-18}
Si-Si	0.0	0.0	0.0

culated so that the zero, first, and second order derivatives of $\mathcal{V}_c^{\mathrm{BKS}}$ and $p(r)$ are equal. The values used for the polynomial coefficients are given in Table II. A graphical representation of this potential is given in Fig. 1.

III. BULK BEHAVIOR OF SiO_2

A. Sample preparation method

The structure of pure silica in the glass phase is that of a disordered network of corner sharing tetrahedra where each silicon is surrounded by four oxygens. The structure of vitreous silica is well known from experimental work.[24–27] The general method for creating a sample of glassy SiO_2 for use in molecular simulation involves gradual cooling of a liquid phase past the liquid to glass transition point.[18,28] The cooling rate is an important parameter as it has been shown that the resulting glass structure is heavily dependent on its creation history.[19] Still, even the slowest cooling rates achievable with today's computers are several orders of magnitude greater than the fastest cooled experimental glasses; as a result much higher glass transition temperatures are expected.[19,21,29] In this study, we have used a method analog to that of Ref. 18 to create a system in the glass phase. The method starts from a β-cristobalite crystal[30] whose density is set to $\rho=2.2$ g/cm^3, the typical density of glassy SiO_2 (Ref. 31). The initial system used here consists of $N=1536$ atoms organized in $4\times4\times4$ crystal cells along the x,y, and z directions. This initial configuration is melted at high temperature ($T=6\times10^3$ K) until all memory from the crystal structure is lost. The fluid phase is then cooled down to $T=300$ K using a series of 13 simulations grouped in sets of three for thermalization, equilibration, and production. Each simulation was 25 ps in length using a time step $\delta t=0.5\times10^{-15}$ s. During the equilibration and production simulations, the temperature was kept constant while during the thermalization simulation, the system was subjected to a temperature gradient where the temperature of the heat bath was decreased every hundred time steps.

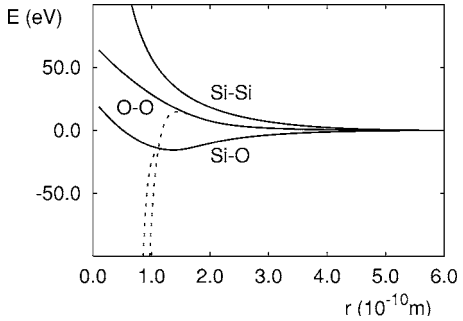

FIG. 1. Graphical representation of the inter-atomic potential. The dashed lines represent the unphysical behavior at short interatomic separations of the original BKS potential.

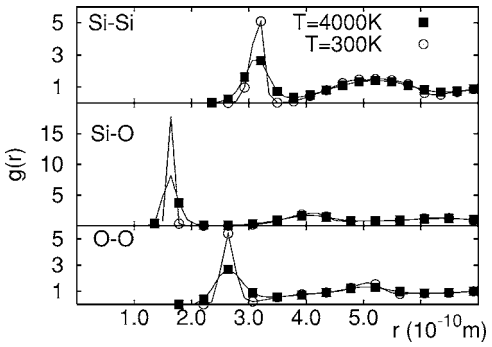

FIG. 2. Representation of the pair correlation functions for the Si-Si(top), Si-O(middle), and O-O(bottom) pairs in the glass phase at $T=300$ K.

B. Analysis

The structure of the glass thus created was assessed by calculating short, medium, and long range structural properties. The long range structure of the glass is obtained through calculation of the pair correlation function as shown in Fig. 2. Short to medium range order is obtained using bond-angle distribution (BAD) (Fig. 3) and ring size analysis (Fig. 4). While we have calculated all six BADs, we restrict ourselves to discussing only the OSiO, SiOSi, and SiSiSi angles distribution (which we will refer to as θ_{OSiO}, θ_{SiOSi}, and θ_{SiSiSi}) as these carry the most information about the structure of the network but also because only θ_{OSiO} and θ_{SiOSi} are available with experimental techniques. Comparison of the results obtained here with those from both experimental and other simulation studies shows good agreement.

Measurements of the $g(r)$ first peak and the location of the bond-length distribution main peak (not shown here) shows that for the O-O, Si-O, and Si-Si pairs we obtain, respectively, $r_{\mathrm{OO}}=2.639$ Å, $r_{\mathrm{SiO}}=1.640$ Å, and $r_{\mathrm{SiSi}}=3.067$ Å. This compares well with the experimental values

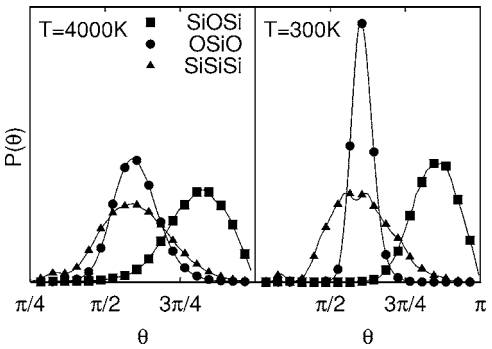

FIG. 3. Bond angle distribution obtained for the Si-O-Si(■), O-Si-O(▲), and Si-Si-Si(•) angles from simulation of the bulk system at both high (left) and low (right) temperatures.

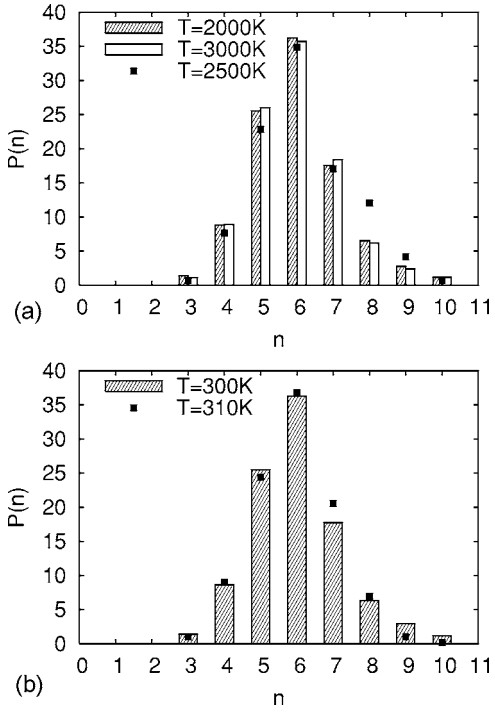

FIG. 4. Ring size distribution measured from the bulk simulations at high (a) and low (b) temperatures. The points (■) represent the results obtained by Rino and Ebbsjö (Ref. 45) at $T=2500$ K and $T=310$ K using the VKRE potential.

$r_{OO}=2.63$ Å and $r_{SiO}=1.61$ Å (Refs. 24 and 26) but also with simulation data.[18,29] Using the BKS potential, Yuan and Cormack[29] found $r_{OO}=2.621$ Å, $r_{SiO}=1.615$ Å, and $r_{SiSi}=3.129$ Å while Vashishta *et al.*[18] obtained $r_{OO}=2.65$ Å, $r_{SiO}=1.62$ Å, and $r_{SiSi}=3.05$ Å using their three-body potential.

The structure of the tetrahedra is measured by the θ_{OSiO} distribution. For a network of perfect tetrahedra, the ideal θ_{SiOSi} is 109.47° close to the experimental value of 109.7°.[32] Simulation data usually reproduce this property well with a value of 108.6°.[22,29] Similarly we obtain 108.9°.

Measurement of the θ_{SiOSi} distribution gives information of the structure beyond the basic tetrahedral configuration. While variations exist, experimental data[24,33–35] suggest a value of 144° for the θ_{SiOSi} distribution peak. Our value of 152° clearly overestimates this, but this seems to be a feature intrinsic to the BKS potential, as the value of 152° and ~150° were reported by other simulation studies.[22,36,37] According to Ref. 36, this can be explained by the lack of Si-O-Si interactions in the cluster model used to derive the BKS potential. In Table III, we present a summary of the above comparisons.

An alternative method to analyze medium range order is the calculation of the n-sized rings distributions. This measures the topology of the SiO_2 network over distances that extend to several Si-O bond distances. Ring size statistics are considered as the generally accepted measure of medium range order in a random-continuous network such as those formed by silicate glasses.[38–41] This allows the identification of topologically different structures. For instance, the ring size distribution is similar for α and β cristobalite or α and β quartz. The distributions however, differ between the two crystal structures, quartz, and cristobalite showing, respectively, single peaks at sizes 6 and 8.

TABLE III. Comparison of the structural properties of the silicate glass obtained with this study and published simulation (Refs. 18, 29, and 36) and experimental (Refs. 24, 26, and 32) results.

	r_{OO}[Å]	r_{SiO}[Å]	r_{SiSi}[Å]	θ_{OSiO}	θ_{SiOSi}
This study	2.639	1.640	3.067	108.9°	152°
24 and 26	2.63	1.61			144°
32				109.47°	
29 and 36	2.621	1.615	3.129	108.6°	152°
18	2.65	1.62	3.05		

In silicon dioxide glass, rings are closed paths where the vertices and edges are, respectively, the Si atoms and the Si-O-Si bonds. Measurement of the ring size distribution is performed using the shortest path analysis[42] which involves identification of the shortest path linking each triplet of first neighbors Si atoms. The number of triplets to consider is related to the Si atom coordination; a four-coordinated Si atom for instance belongs to six different rings. The difficulty of the ring size analysis lies in defining a unique criteria able to identify the primitive rings, i.e., those rings which are not formed by the combination of smaller rings. It has been shown that simply counting all rings up to a given size leads to meaningless results.[38,39,41] The number of rings increasing monotonously with ring size as small rings are counted several times as part of bigger rings. A correct ring analysis must therefore identify exclusively primitive rings.

In this study we choose to use the criteria based on those proposed by Franzblau[43] and Marians and Hobbs[44] for the definition of a primitive ring.

The first step is to build the network connectivity. The common approach to this is to count as a bond all distances shorter than a given threshold. As we plan to study highly densified shocked phases, this method can however, lead to an unrealistically large number of bonds and therefore we have chosen an alternative method.

A neighbor list is built for each atom to identify all Si_i-O_j bonds. Care must be taken that this method is reversible, i.e., the path $Si_1-O_2-Si_2$ must exist both in the Si_1 and Si_2 neighbor lists. A successful method to build those lists is to loop over all O_i and find $Si_{i,1}$ and $Si_{i,2}$, the two closest Si neighbors. O_i then registers itself in the neighbor list of $Si_{i,1}$ and $Si_{i,2}$. Although this method assumes that each oxygen has a twofold coordination, it can be shown that the connectivity obtained with this method is consistent with the network topology and allows to recover an accurate Si coordination.

The next step is to identify all candidate rings. This is done by triple looping over all Si_i atoms and all their first Si_1 and Si_2 neighbors. For each (Si_i, Si_1) pair, we build a tree of all successive neighbors of Si_1 down to the eleventh level and identify the position of Si_2. The candidate rings are the Si_i-Si_1-$\cdots$-Si_2 closed paths in the tree.

Each candidate ring is then tested against our shortest-path criteria. This criteria follows the definition given by Franzblau.[43] A n-member ring is considered as primitive if

by following the $Si_0, Si_1, \ldots, Si_i, \ldots, Si_n$ atoms which form the ring, the Si_0-Si_i distance sequence is unimodal. This criteria allows one to remove all rings whose shape is not convex such as eight-shaped or tennis racket-shaped rings. The shortest ring isolated as such is counted in the statistics.

The method has been tested against both β and α-cristobalite crystals and leads to a distribution with only six-membered rings. Figure 4 shows the ring size distribution obtained from the bulk simulations at both high and low temperatures along with a comparison with the results obtained by Rino and Ebbsjö[45] using the VKRE model. Unfortunately they did not provide any details regarding the shortest-path criteria used in their study. Save for a discrepancy for eight-membered rings at high temperature, Fig. 4 shows good agreement between the two studies.

IV. SiO_2 UNDER SHOCK CONDITIONS

A. Method

The analysis of shock-induced structural changes have been investigated using a nonequilibrium molecular dynamics method. The initial system of size $N=30\times10^3$ atoms consisted of $50\times5\times5$ β-cristobalite cells along the x, y, and z directions. Periodic-boundary conditions were applied along the y and z axes while free surfaces were used along x. The method described in the previous section was applied to this initial configuration to obtain a glass phase. All shock simulation started from a well equilibrated glass system at $T=300$ K.

At $t=t_0$, the system was hit by two pistons represented by (y,z) planes of infinite mass on the left- and right-hand surfaces. The left piston has a velocity $u\neq0$ along positive x while the piston on the right-hand side had a zero velocity. Displacement of the left-hand side piston induced the propagation of a mechanical shock wave through the sample whose velocity D is a function of u and of the equation of state of the system. The shock wave divides the system in two parts: the nonshocked region, which is located downstream of the shock wave, is referred by the subscript 0 while the shocked region, located upstream of the shock wave, is referred by the subscript 1. The aim here is to analyze the shock-induced structural changes in the shocked region.

B. Analysis

Analysis of the shocked region is performed using a moving analysis window whose size and position changes with time so as to match that of region 1. The dimensions of this window are calculated using the profile of particle velocity along x, the shock propagation direction. The shock front is located using the point of maximum inflexion on the profile. The shocked and nonshocked regions are located, respectively, up and downstream of this point and separated by a transition region where the system undergoes the near-instantaneous transition from unshocked to shocked states. This transition region is identified using a numerical algorithm that analyzes local variations in the profile and excluded from the analysis window. The thermodynamic, structural, and topological properties are then computed independently in each region.

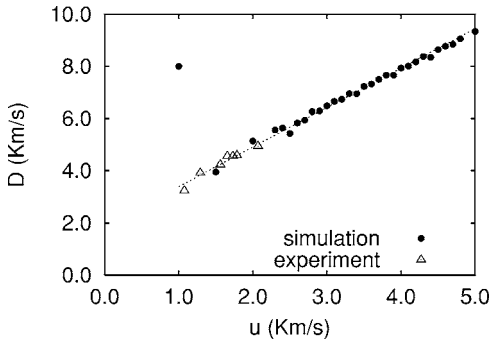

FIG. 5. Evolution of the shock velocity (D) as a function of piston velocity (u) as obtained from the nonequilibrium shock simulations. The dotted line represents the linear fit of the simulation data. Experimental data are taken from Ref. 46.

Measurement of the shock front position as a function of time and for each piston velocity allows one to measure $D(u)$ as shown on Fig. 5. In the plastic regime, the curve obtained here is very similar to that of Ref. 6. For $D>1$ Km/s the system undergoes a transformation from an elastic to plastic regime where u is a linear function of D. In the latter regime, we observe shock-induced structural changes and a permanent densification of the system. Additionally, our curve compares well with the experimental data obtained by Sugiura *et al.*[46] using a flier plate experiment.

We, however, note a difference between our data and those of Ref. 6 in the elastic regime. This is a consequence of our analysis algorithm which uses the velocity profile to locate the shock front position. In the elastic regime, the small changes induced to the velocity profile lead to a very noisy measurement of the shock front position as a function of time; hence the difference in the shock velocity. This behavior disappeared however, as the plastic regime, which is of interest here, is entered.

Figure 6 shows the shock-induced modifications of the bond-angle distributions. Upon increasing the shock velocity, the distributions gradually change from that of an unshocked material to that of a heavily shocked material. For the θ_{OSiO} distribution, this involves displacement of the main peak to lower angles, indicating a reduction of the average tetrahedra size which is compatible with the shock-induced densification. The stronger the shock, the more dense the phase and therefore the smaller the average tetrahedra. This is consistent with experimental observation of the variation of θ_{OSiO} under pressure.[47,48]

Variations of the θ_{SiOSi} distribution obeys the same rule, stronger shock waves induce smaller angles which corresponds to a denser phase. We however, note the creation of a local maxima at $\theta_{SiOSi}=105.30°$ for intermediate shock strengths. Again, the same phenomenon has been observed experimentally.[49,50] The θ_{SiSiSi} distributions of the unshocked material shows two peaks at $\theta^1_{SiSiSi}=60.30°$ and $\theta^2_{SiSiSi}=103.50°$ with a much higher probability for θ^2_{SiSiSi} ($\theta^2_{SiSiSi}/\theta^1_{SiSiSi}=12.03$). In the shocked materials, while the positions of the peaks shift only slightly to lower and greater angles for, respectively, θ^1_{SiSiSi} and θ^2_{SiSiSi}, their ratios near

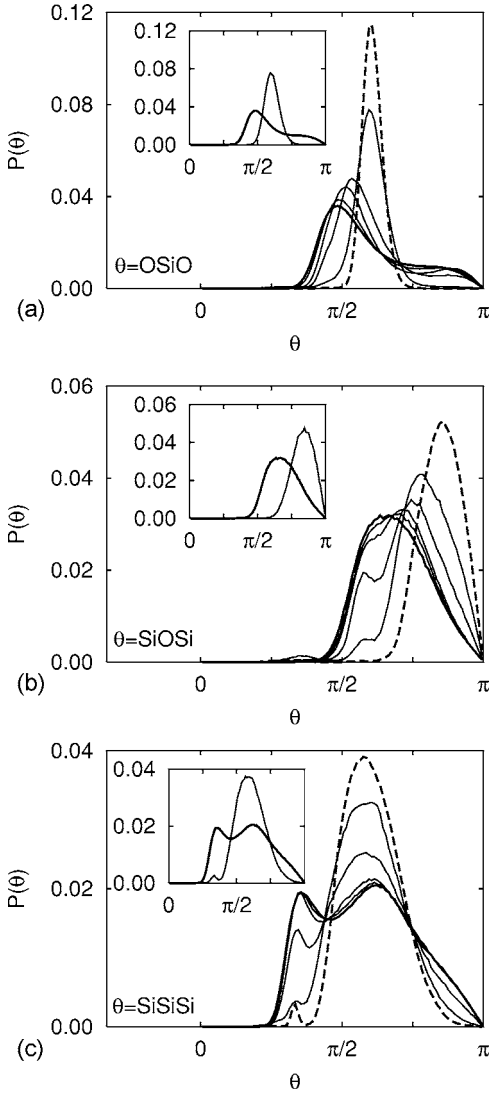

FIG. 6. Shock-induced modifications of the θ_{OSiO} (a), θ_{SiOSi}(b), and θ_{SiSiSi} (c) bond angle distributions. In the main graphs the dashed curves represent the distributions of the unshocked materials and the bold line the distributions for the highest shock velocities (v_p=4.5 Km/s). The solid lines represent the distributions for v_p =1,2,3.5,4,4.5 Km/s. The insert shows a comparison between the high shock velocity distribution (bold line) and those obtained from an unshocked bulk system with similar temperature (T=2000 K).

one for the fastest shock velocities used here. The shift of the $\theta^1_{\mathrm{SiSiSi}}$ peak to lower angles is understandable from the densification of the materials, which induces the intertetrahedra angle to decrease. The shift of the $\theta^2_{\mathrm{SiSiSi}}$ peak to higher angles is however, counterintuitive as this corresponds to an opening of the intertetrahedra angle, which is not *a priori* compatible with the phase densification. In terms of the system's topology, the shifts to lower angles of the $\theta^1_{\mathrm{SiOSi}}$ and $\theta^1_{\mathrm{SiSiSi}}$ distribution peaks suggests an increase of small ring while the shift of $\theta^2_{\mathrm{SiSiSi}}$ to higher angles also suggests an increase in the proportion of large rings.

The inserts of Fig. 6 compare the distributions obtained for the fastest shock velocity used here with those obtained from bulk simulations at a temperature equal to that found in

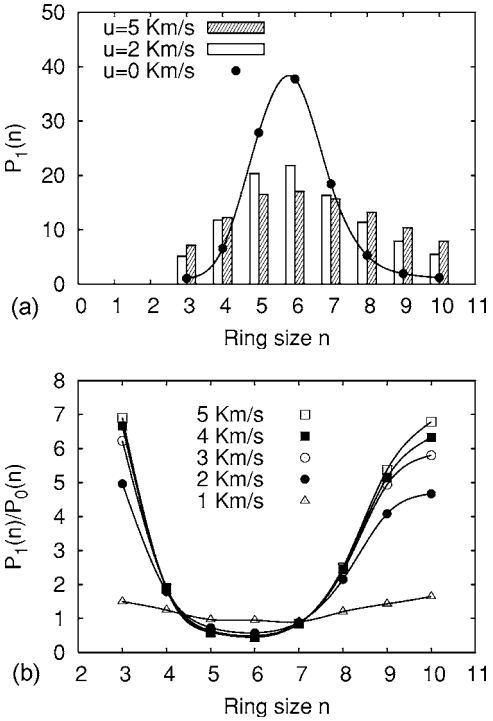

FIG. 7. Ring size distribution in the shocked materials. Subfigure (a) compares the distribution in the unshocked region with those in the shocked region with slow and fast piston velocity. Subfigure (b) represents the ring size proportion in the shocked region for different u divided by the proportion in the unshocked region.

the shocked region. This shows that the structure of the shocked state is much different than that of a high temperature system. The modifications observed here are therefore induced by the propagation of the shock wave and not merely the consequence of the associated temperature increase. The θ_{OSiO} distribution suggests a reduction of the average tetrahedra size whereas the modifications of the θ_{SiOSi} and θ_{SiSiSi} distributions suggest an increase in the proportion of both small and large rings.

In order to further assess the medium-range structure modification induced by the shock wave, we compare the ring size histograms in the shocked and unshocked regions. In agreement with the results of Ref. 5, Fig. 7(a) confirms the results suggested by the bond-angle distributions. As the shock velocity increases, the ring size distribution in the shocked regions flattens out suggesting a structural reorganization which translates into an increase of both small (3–4) and large (7–10) rings. Observation of the ratio of the rings size proportion in the shocked region to that in the unshocked region shows that the relative increase is similar for both sizes. While the increase in the proportion of small rings is easily understandable considering the shock induced densification of the material, the increase of the large ring is less so. One would assume that reducing the average ring size and the average θ_{SiOSi} would favor small rings only. The increase in the proportion of large ring can be related to the θ_{SiSiSi} distribution. This indicates that the system favors two configurations with an intertetrahedra angle of about 60° and 100°. The low angle peak accounts for the small rings while

the high angle peak accounts for large rings. Experimentally, it has been shown that the presence of three and four membered Si rings in silicate glass can be associated to the so-called D_2 and D_1 peaks respectively, in Raman spectra.[51] The shock induced intensity increase of the D_2 and D_1 peaks in the Raman spectra of Okuno *et al.*[50] thus confirms our simulation data. Unfortunately, a similar connection cannot be made for large rings as they cannot be precisely isolated experimentally.

V. MODELING SiO_2 USING THE HUGONIOSTAT

A. Method

As an alternative method to nonequilibrium molecular dynamics which involves the simulation of large systems, we seek here to simulate the shock induced structural changes using bulk simulations in the Hugoniot ensemble. The advantage of using such a method is that it requires fewer atoms $[\mathcal{O}(10^3)]$ which allows one to run much longer simulations and achieve better statistics in shorter simulation times. Here we use the GNVHug Hugoniostat of Soulard[11] as it allows to reach equilibrium very quickly and obeys the Hugoniot relations at all times. The method has been applied successfully to the computation of the Hugoniot in the solid and liquid phases; the behavior of the method in the glassy state remains unknown, however. According to its original phase, a material uses very different thermodynamic paths in the near-instantaneous transition to the shocked state and therefore successful application of the GNVHug method in one phase does not translate to another. We therefore also aim to clarify the issue of the applicability of the GNVHug method to glassy phases.

The GNVHug has been described in detail in previous publications.[11,12] We recall here the general idea.

A cubic system whose size L and volume V are allowed to vary with time is considered with three-dimensional periodic boundary conditions applied. The system consists of N atoms i with individual masses m_i, and E_p, and E_k the total potential and kinetic energies. Using the Gauss principle,[52–54] the time evolution of the system is such that

$$\frac{1}{2}\sum_{i=1}^{N}\left(m_i\left[\frac{f_i}{m_i}-\frac{d^2r_i}{dt^2}\right]^2\right) \tag{3}$$

with $f_i=-\partial E_p/\partial r_i$, is minimum at all times.

Given a volume V, the system is constrained on the thermodynamic hypersurface $H(E,P)$ which corresponds to a Hugoniot state at thermodynamic equilibrium:

$$H=E-\frac{1}{2}P(V_0-V)=E_0+\frac{1}{2}P_0(V_0-V) \tag{4}$$

with P_0, E_0, and V_0 the initial pressure, energy, and volume and P and E the pressure and the energy behind the shock. The pressure is defined using the virial expression:

$$P=\frac{Nk_BT}{V}+\frac{\Phi}{3V}, \tag{5}$$

where Φ is the virial and k_B the Boltzmann constant.

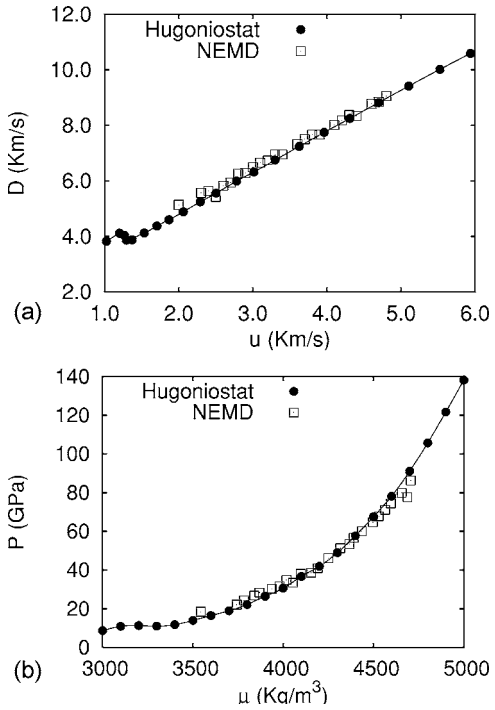

FIG. 8. Comparisons of the thermodynamic properties obtained with the NEMD (□) and Hugoniostat (•) methods.

Since V is taken to be constant (i.e., $\frac{dV}{dt}=0$) we get:

$$\frac{dE}{dt}-\frac{1}{2}\frac{dP}{dt}(V_0-V)=0. \tag{6}$$

Combining Eqs. (3) and (6) *via* a Lagrange multiplier λ, the following equation of motions is obtained:

$$\frac{d^2r_i}{dt^2}=\frac{f_i}{m_i}-\lambda\frac{dr_i}{dt}, \tag{7}$$

$$\lambda=\frac{V-V_0}{4V-V_0}\frac{\frac{1}{2}\frac{d\Phi}{dt}+\sum_i^N f_i\frac{dr_i}{dt}}{2E_k}. \tag{8}$$

The first stage of the Hugoniot calculation involves the determination of P_0 and E_0 by means of standard molecular dynamics simulations in the canonical ensemble. The GNVHug algorithm is then started by scaling the system to a chosen volume V. The initial positions of atoms are deduced from the initial structure and the appropriate scale factor $(V/V_0)^{(1/3)}$. Knowing the virial and the potential energy, the relevant kinetic energy is calculated so as to satisfy Eq. (4). If a negative value is obtained, the system is relaxed for a few hundred time steps until the kinetic energy becomes positive.

B. Results

In order to test the GNVHug method, a glass system was prepared using the method described in Sec. III. The initial configuration was a β-cristobalite crystal of $N=1536$ atoms ($4\times4\times4$ crystal cells) with three-dimensional periodic

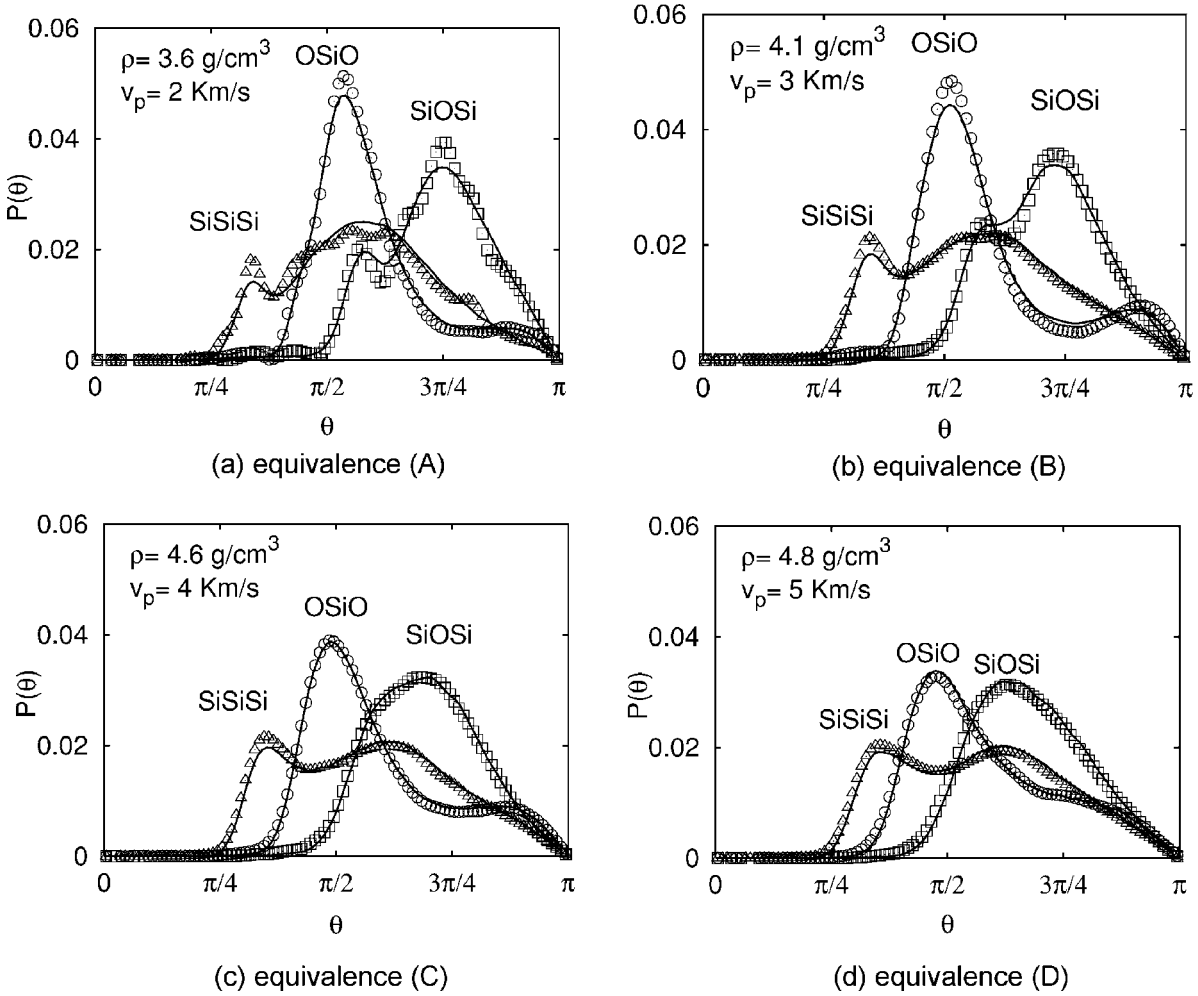

FIG. 9. Comparison of the bond angle distributions measured using the NEMD and the Hugoniostat method for several equivalent densities and shock velocities in the plastic regime. The points represent the Hugoniostat results while the lines and histograms show the shock data.

boundary conditions applied. All simulations in the Hugoniot ensemble started from the same, well equilibrated glass system. The pole parameters (E_0, P_0, V_0) which are required as input parameters for the simulations were averaged over the last production simulation of the glass preparation procedure. Shock densities in the range $\rho_1 \in [3:5]\mathrm{g/cm}^3$ were used.

The first comparison between the NEMD and GNVHug methods involves the calculation of the shock wave velocity as a function of piston velocity $[D(u)]$ and the calculation of the Hugoniot equation of state $[P_1(\rho_1)]$. Direct comparison between the two methods is, however, not possible as some parameters of one method (e.g., D) are not directly accessible in the second. We therefore make use of the Hugoniot relations to be able to compare the results obtained from the two methods. From the fundamental Hugoniot relations[55] one can derive:

$$\rho_1 = (\rho_0 D)/(D-u), \tag{9}$$

$$P_1 = \rho_0 D u + P_0, \tag{10}$$

$$D = \rho_0^{-1}\sqrt{(P_1 - P_0)/(\rho_0^{-1} - \rho_1^{-1})}, \tag{11}$$

$$u = \sqrt{(P_1 - P_0)(\rho_0^{-1} - \rho_1^{-1})}. \tag{12}$$

Using Eqs. (9)–(12), Fig. 8 shows the comparison of $D(u)$ and $P_1(\rho_1)$ obtained using the two methods. This shows that the thermodynamic quantities are in very close agreement in the plastic regime. The elastic regime is in principle also available to the Hugoniot method as it obeys the Hugoniot relations. However, for small density increments, the shock-induced effects are reversible and the shocked state differs little from the unshocked state; hence $H \sim 0$. Constraining the system to $\frac{\partial H}{\partial t} = 0$ is therefore a numerically challenging task which explains why the method fails to match the NEMD results in the elastic regime. This does not question the efficiency of the method, but is merely a numerical flaw of the glassy systems used. Additionally, as an amorphous glassy phase is studied here, it is assumed that anisotropic effects are negligible and therefore we have only computed the pressure and not the shear stress as the approximation of isostatic should hold.

Figures 9 and 10 show the comparison of the structural properties between the NEMD and Hugoniot methods. Using

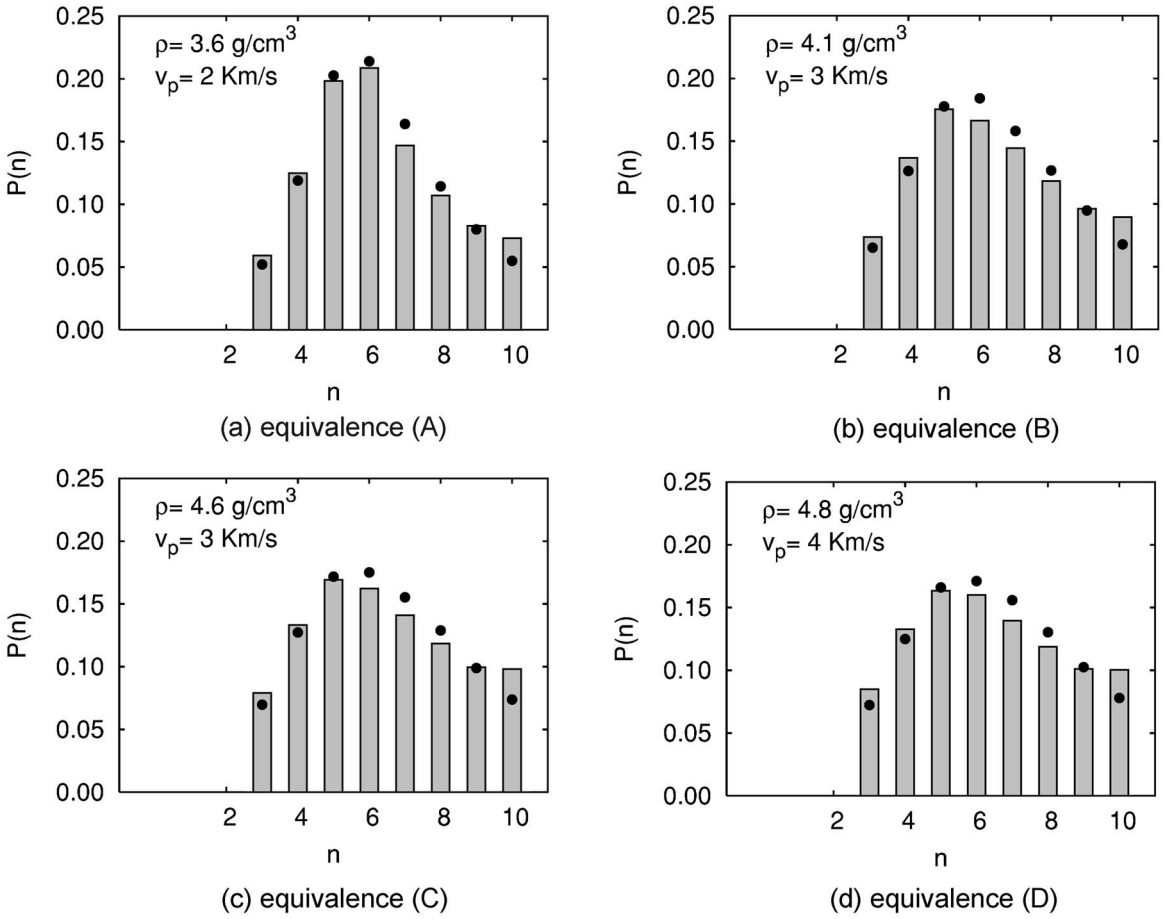

FIG. 10. Comparison of the ring-size distributions measured using the NEMD and the Hugoniostat method for several equivalent densities and shock velocities in the plastic regime. The points represent the Hugoniostat results while the lines and histograms show the shock data.

the results of Fig. 8, the following parameters are taken to lead to equivalent conditions:

$$(\mathrm{A}):\rho = 3.6\ \mathrm{g/cm^3} \leftrightarrow v_p = 2\ \mathrm{Km/s},$$

$$(\mathrm{B}):\rho = 4.1\ \mathrm{g/cm^3} \leftrightarrow v_p = 3\ \mathrm{Km/s},$$

$$(\mathrm{C}):\rho = 4.6\ \mathrm{g/cm^3} \leftrightarrow v_p = 4\ \mathrm{Km/s},$$

$$(\mathrm{D}):\rho = 4.8\ \mathrm{g/cm^3} \leftrightarrow v_p = 5\ \mathrm{Km/s}.$$

Computation of both the bond-angle distributions and the ring-size distributions show very close agreement in the structures obtained with the equilibrium and nonequilibrium simulations. For simulation equivalents to piston velocities greater than 3 Km/s, the two sets of results become virtually indistinguishable. This shows that past the plastic regime limit, the shock-induced structural properties are available using the equilibrium method.

The main advantage of using the GNVHug method here lies in the speed with which the results were obtained. Starting from a β-cristobalite crystal, the creation of the (large) glass sample and the shock simulations required more than a month of computation using parallel simulations with six processors. Using the same resources and single processor calculations, the Hugoniostat method required a mere week of simulation to recover the same results. Besides the clear financial advantage of using short simulations, this opens up the prospect of using more realistic methods and potentials. The small system sizes and three-dimensional periodicity associated with the GNVHug method make usage of long-range Coulombic interactions with dynamic charges and many-body potentials a standard exercise. Application of a similar method with direct shock propagation, while possible, is much more complicated. The system size and complicated boundaries require more complicated techniques for treatment of the long-range forces (i.e., fast multipole method) in addition to large computational overheads.

VI. CONCLUSION

In this paper we have used atomistic simulations to model the shock-induced structural changes in silicate glass. Our model is a modified version of the BKS potential where the long-range part of the interaction is cut and shifted, based on the assumption that the glass structure is mainly dictated through interactions within the first neighbor shell. We show that the glass produced with this potential is structurally

equivalent to those generated using the BKS potential with long range interaction and the three-body VKRE potential. In addition, our structural parameters are consistent with those found in experimental studies. This therefore suggests the validity of the assumption made here. The short range interactions are responsible for the average tetrahedra size and shape as well as their relative positions. The glass being a continuous random network of connected tetrahedra, the long range order is controlled by the cumulative effects of setting the individual tetrahedra structure and their relative positions with respect to their immediate neighbors.

We have subsequently used nonequilibrium molecular dynamics to propagate mechanical shock waves through our glassy system. Comparison of the structures measured in the shocked and unshocked regions reveal that, above the plastic regime limit, the shock wave induces profound and irreversible structural changes. These are manifested by the reduction in the average tetrahedra size associated with the material densification. The relative positions of the tetrahedra is distributed with equal probabilities among two configurations where the angle made by connected tetrahedra equals 60° or 103°. Analysis of the ring size distributions shows that this is connected with an increase in the proportion of both 3–4 and 7–10 membered rings. Thus, in addition to the material densification manifested by smaller tetrahedra and narrow intertetrahedra angles, the shock wave also stabilizes the formation of large rings in the network created by wide intertetrahedra angles.

We have then applied the GNVHug Hugoniostat method to perform equilibrium bulk simulations of the shock-induced structural changes. The method is shown to reproduce well the $D(u)$ and $P_1(\rho_1)$ curves in the plastic regime. Analysis of the structures shows very good agreement with those obtained using NEMD simulations; the correspondence improving with increased shock wave velocities. As the Hugoniostat method allows use of much smaller systems, these results open up the prospect of achieving modeling of the shock wave induced effects using complicated potentials at a fraction of the cost required to run large scale shock simulations.

This will form the basis of future work where the Hugoniostat method will be used to explore more complicated potentials including long-range forces and dynamics charges but also more complicated setups in an attempt to obtain a more realistic model of the mechanisms underlying damage of the optics by high-power lasers. Additionally, the results obtained from the bulk simulation will be completed by a more refined study to quantify the influence of long-range forces on the structural properties of the glass comparing the glass structure obtained with and without treatment of the long range forces.

[1] M. D. Feit, J. H. Campbell, D. R. Faux, F. Y. Gening, M. R. Kozlowski, A. M. Rubenchik, R. A. Riddle, A. Salleo, and J. Yoshiyama, Proc. SPIE **3244**, 350 (1997).

[2] M. D. Feit, L. W. Hrubesh, A. M. Rubenchik, and J. N. Wong, Proc. SPIE **4347**, 316 (2000).

[3] S. G. Demos, M. R. Koslowski, M. Staggs, L. L. Chase, A. Burnham, and H. B. Radousky, in *32nd Annual Symposium on Optical Materials for High Power Lasers*, 2000.

[4] H. Sugiura, R. Ikeda, K. Kondo, and T. Yamadaya, J. Appl. Phys. **81**, 1651 (1996).

[5] A. Kubota, M.-J. Caturla, J. S. Stolken, and M. D. Feit, Opt. Express **8**, 611 (2001).

[6] A. Kubota, M.-J. Caturla, J. S. Stolken, B. Sadigh, A. Quong, A. Rubenchik, and M. D. Feit, Proc. SPIE 2003.

[7] S. Susman, K. J. Volin, D. L. Price, M. Grimsditch, J. P. Rino, R. K. Kalia, P. Vashishta, G. Gwanmesia, Y. Wang, and R. C. Liebermann, Phys. Rev. B **43**, 1194 (1991).

[8] K. Trachenko and M. Dove, J. Phys.: Condens. Matter **14**, 7449 (2002).

[9] L. P. Dávila, M. J. Caturla, A. Kubota, B. Sadigh, T. Diaz dela Rubia, J. F. Shackelford, S. H. Risbud, and S. H. Garofalini, Phys. Rev. Lett. **91**, 205501 (2003).

[10] V. V. Zhakhovskiĭ, S. V. Zybin, K. Nishihara, and S. I. Anisimov, Phys. Rev. Lett. **83**, 1175 (1999).

[11] L. Soulard, *Shock Compression of Condensed Matter*, 1999.

[12] L. Soulard, *Shock Compression of Condensed Matter*, 2001.

[13] J.-B. Maillet, M. Mareschal, L. Soulard, R. Ravelo, P. S. Lomdahl, T. C. Germann, and B. L. Holian, Phys. Rev. E **63**, 016121 (2000).

[14] S. Bernard and J.-B. Maillet, Phys. Rev. B **66**, 012103 (2002).

[15] R. Ravelo, B. L. Holian, T. C. Germann, and P. S. Lomdahl, Phys. Rev. B **70**, 014103 (2004).

[16] Y. Limoge, Acad. Sci., Paris, C. R. **4**, 263 (2001).

[17] B. W. H. van Beest, G. J. Kramer, and R. A. van Santen, Phys. Rev. Lett. **64**, 1955 (1990).

[18] P. Vashishta, R. K. Kalia, J. P. Rino, and I. Ebbsjö, Phys. Rev. B **41**, 12197 (1990).

[19] W. Kob, K. Vollmayr, and K. Binder, Phys. Rev. B **54**, 15808 (1996).

[20] Y. Guissani and B. Guillot, J. Chem. Phys. **104**, 7633 (1996).

[21] B. Coluzzi and P. Verrocchio, J. Chem. Phys. **116**, 3789 (2002).

[22] P. Jund, M. Rarivomanantsoa, and R. Julien, J. Phys.: Condens. Matter **12**, 8777 (2000).

[23] J. D. Halverson and F. Barmes (unpublished).

[24] R. L. Mozzi and B. E. Warren, J. Appl. Phys. **2**, 164 (1969).

[25] R. Brückner, J. Non-Cryst. Solids **5**, 123 (1970).

[26] P. A. V. Johnson, A. C. Wright, and R. N. Sinclair, J. Non-Cryst. Solids **58**, 109 (1983).

[27] A. C. Wright, J. Non-Cryst. Solids **179**, 84 (1994).

[28] J. Horbach and W. Kob, Phys. Rev. B **60**, 3169 (1990).

[29] X. Yuan and A. N. Cormack, J. Non-Cryst. Solids **283**, 69 (2001).

[30] W. G. Wickoff, *Crystal Structures*, 2nd ed. (Wiley, New York 1963).

[31] *Handbook of Chemistry and Physics*, edited by R. C. Weast (The Chemical Rubber Co., Cleveland, OH, 1970).

[32] D. J. Grimley, A. C. Wright, and R. C. Sinclair, J. Non-Cryst. Solids **119**, 49 (1990).

[33] S. V. Nemilov, Fiz. Khim. Stekla **8**, 385 (1982).

[34] P. G. Coombs, J. F. De Natale, P. J. Hood, D. K. McElfresh, R. S. Wortman, and J. F. Shackelford, Philos. Mag. B **51**, L39 (1985).
[35] F. L. Galeener, Philos. Mag. B **51**, L1 (1985).
[36] X. Yuan and A. N. Cormack, J. Non-Cryst. Solids **319**, 31 (2003).
[37] P. Jund and R. Julien, Philos. Mag. A **39**, 37 (1999).
[38] D. Weaire and F. Wooten, J. Non-Cryst. Solids **35-36**, 495 (1980).
[39] A. Tadros, M. A. Klenin, and G. Lucovsky, J. Non-Cryst. Solids **75**, 407 (1985).
[40] J. M. Greneche, J. Teillet, and J. M. D. Coey, J. Non-Cryst. Solids **83**, 27 (1985).
[41] W. D. Luedtke and U. Landman, Phys. Rev. B **40**, 1164 (1989).
[42] A. C. Wright and J. A. E. Desa, Phys. Chem. Glasses **19**, 140 (1978).
[43] D. S. Franzblau, Phys. Rev. B **44**, 4925 (1991).
[44] C. S. Marians and L. W. Hobbs, J. Non-Cryst. Solids **124**, 242 (1990).
[45] J. P. Rino, I. Ebbsjö, R. K. Kalia, A. Nakano, and P. Vashishta, Phys. Rev. B **47**, 3053 (1993).
[46] H. Sugiura, K. Kondo, and A. Sawaoka, J. Appl. Phys. **52**, 3375 (1981).
[47] R. A. B. Devine and J. Arndt, Phys. Rev. B **35**, 9376 (1987).
[48] R. A. B. Devine, R. Dupree, I. Farnan, and J. J. Capponi, Phys. Rev. B **35**, 2560 (1987).
[49] R. J. Hemley, H. K. Mao, P. M. Bell, and B. O. Mysen, Phys. Rev. Lett. **57**, 747 (1986).
[50] M. Okuno, B. Reynard, Y. Shimada, Y. Syono, and C. Willaime, Phys. Chem. Miner. **26**, 304 (1999).
[51] A. Pasquarello and R. Car, Phys. Rev. Lett. **80**, 5145 (1998).
[52] W. G. Hoover, *Molecular Dynamics* (Springer-Verlag, Berlin, 1986).
[53] D. J. Evans, W. G. Hoover, B. H. Failor, B. Moran, and A. J. C. Ladd, Phys. Rev. A **28**, 1016 (1983).
[54] G. P. Morris and C. P. Dettmann, Chaos **8**, 321 (1998).
[55] J. Thouvenin, *Détonique* (Eyrolles, Paris, 1997).